# <sup>3</sup>Trends in Northern Hemispheric Snow Presence

YISU JIA<sup>®</sup>, ROBERT LUND, JIAJIE KONG, JAMIE DYER, JONATHAN WOODY, AND J. S. MARRON<sup>®</sup>

<sup>a</sup> Department of Mathematics and Statistics, University of North Florida, Jacksonville, Florida <sup>b</sup> Department of Statistics, University of California, Santa Cruz, Santa Cruz, California

<sup>c</sup> Department of Geosciences, Mississippi State University, Mississippi State, Mississippi

<sup>d</sup> Department of Mathematics and Statistics, Mississippi State University, Mississippi State, Mississippi
<sup>e</sup> Department of Statistics and Operations Research, University of North Carolina at Chapel Hill, Chapel Hill, North Carolina

(Manuscript received 19 September 2022, in final form 29 March 2023, accepted 30 March 2023)

ABSTRACT: This paper develops a mathematical model and statistical methods to quantify trends in presence/absence observations of snow cover (not depths) and applies these in an analysis of Northern Hemispheric observations extracted from satellite flyovers during 1967–2021. A two-state Markov chain model with periodic dynamics is introduced to analyze changes in the data in a cell by cell fashion. Trends, converted to the number of weeks of snow cover lost/gained per century, are estimated for each study cell. Uncertainty margins for these trends are developed from the model and used to assess the significance of the trend estimates. Cells with questionable data quality are explicitly identified. Among trustworthy cells, snow presence is seen to be declining in almost twice as many cells as it is advancing. While Arctic and southern latitude snow presence is found to be rapidly receding, other locations, such as eastern Canada, are experiencing advancing snow cover.

SIGNIFICANCE STATEMENT: This project quantifies how the Northern Hemisphere's snow cover has recently changed. Snow cover plays a critical role in the global energy balance due to its high albedo and insulating characteristics and is therefore a prominent indicator of climate change. On a regional scale, the spatial consistency of snow cover influences surface temperatures via variations in absorbed solar radiation, while continental-scale snow cover acts to maintain thermal stability in the Arctic and subarctic regions, leading to spatial and temporal impacts on global circulation patterns. Changing snow presence in Arctic regions could influence large-scale releases of carbon and methane gas. Given the importance of snow cover, understanding its trends enhances our understanding of climate change.

KEYWORDS: Changepoint analysis; Regression analysis; Statistical techniques; Statistics; Time series

### 1. Introduction

Snow cover plays a critical role in Earth's hydrological processes and its impact on the broader global climate is of great interest (Barnett et al. 2005; Karl et al. 2009; Goudie 2018; van Mantgem et al. 2009). Snow greatly influences the global energy balance due to its high albedo and insulating characteristics and is therefore a prominent indicator of climate change (Liston and Hiemstra 2011; Mote 2003; Lawrence and Slater 2010; Callaghan et al. 2011). On a regional scale, the spatial consistency (patchiness) of snow cover can influence surface temperatures via horizontal variations in absorbed solar radiation. Continental-scale snow cover acts to maintain thermal stability in the Arctic and subarctic regions, possibly inducing changes in global circulation patterns attributable to large-scale releases of carbon and methane gas (Zona et al. 2015). While the amount of water available in the snowpack is quantified in snow depths and/or snow water equivalents (SWE), areal snow presence/coverage defined by snow cover extent (SCE) is often used to estimate the location

Oenotes content that is immediately available upon publication as open access.

Corresponding author: Yisu Jia, y.jia@unf.edu

and availability of regional water resources (Mote et al. 2018; Serreze et al. 2000; Robinson et al. 1993).

Remotely sensed satellite images are common sources of SCE data; these images provide spatial and temporal observations that can be used in regional and continental-scale analyses. Satellite data are used here to estimate SCE trends, allowing us to assess SCE changes over time and space. The satellite-derived SCE data product investigated here is binary, with snow presence being recorded as unity and snow free ground being assigned zero.

Some midlatitude locations have sporadic snow coverage, with snow cover typically lasting only a few weeks at a time, even during the height of winter. The majority of our work lies with introducing a mathematical model and developing the statistical methods needed to analyze trends in autocorrelated and binary-valued sequences. The model is flexible enough to adapt to the data from many of our study cells.

Statistical analysis of snow data has been debated in the climate literature, especially in regard to trend and uncertainty assessment (see Yue et al. 2002, and the references therein). Here, a flexible mathematical model and rigorous accompanying statistical methods are used to estimate trends and accurately assess their uncertainty margins. Some nuances arise in this pursuit. First, as our SCE data are recorded weekly, annual periodicity needs to be taken into account. Second, since SCE data are correlated, with snow presence in a week making snow presence in adjacent weeks more likely, serial autocorrelation needs to be

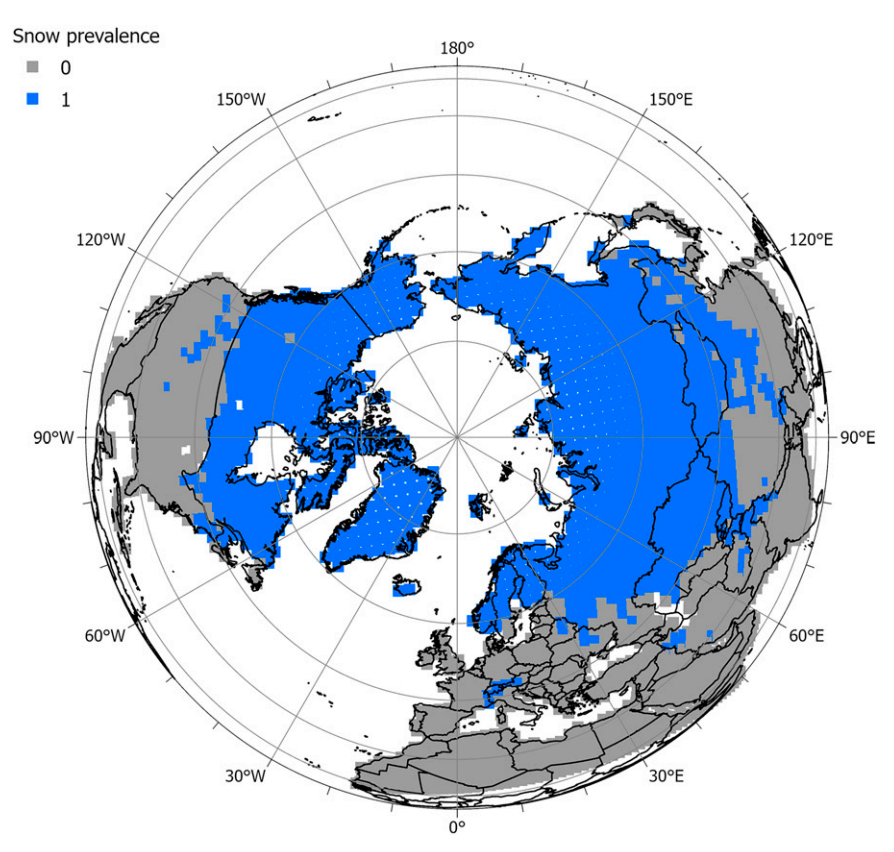


FIG. 1. NH snow coverage reported by the NH Weekly Visible Satellite Charts (Robinson et al. 2012) for the week of 1–7 Dec 2020.

accounted for in trend uncertainty quantifications. Finally, previous authors have noted data quality issues (Bormann et al. 2018; Estilow et al. 2015) in some cells that need to be addressed, without pinpointing the specific problematic cells. We carefully address this issue below. The general pattern of results found here agrees with trends found in other studies using more rudimentary statistical approaches (Brown and Robinson 2011; Lemke et al. 2007; Notarnicola 2022).

The rest of this paper proceeds as follows. Section 2 describes the SCE data used in this study and their nuances. Section 3 introduces the mathematical model and statistical methods needed to quantify the problem, including the all-important uncertainty calculations for our trend estimates. Section 4 presents a simulation study, showing that model parameters can be accurately estimated from a half-century of weekly observations. Section 5 presents two case studies, analyzing observations from a cell in North Dakota that is actually experiencing increasing snow coverage. We also give an example of data from a cell having poor data quality. Section 6 presents results for the entire Northern Hemisphere (NH) and discusses our general findings and their implications. Section 7 concludes with comments and remarks.

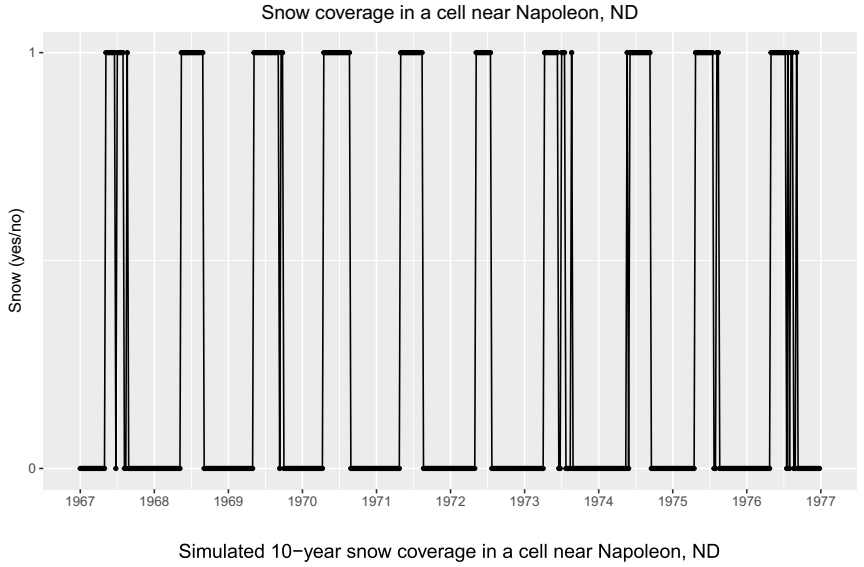
#### 2. Data

The data studied here were aggregated from daily satellite flyovers, with SCE values being estimated manually weekly by meteorologists for each study cell. Specifically, this study uses the Northern Hemisphere Weekly Visible Satellite Charts data from the Climate Data Record as developed by the National Oceanic and Atmospheric Administration (NOAA) (Robinson et al. 2012). The data are available at https://www.ncei.noaa.gov/access/metadata/landing-page/bin/iso?id=gov.noaa.ncdc: C00756.

The Rutgers University Snow Laboratory at http://climate.rutgers.edu/snowcover/ was an integral part of the construction of the data product studied here and is a useful repository for literature and links to this and other SCE datasets. This study examines the time period August 1967–July 2021. For cell structure, the data use NOAA's  $89 \times 89$  Cartesian grid that overlies a polar stereographic projection of the NH. The product contains  $88 \times 88 = 7744$  cells with a resolution of 190.4 km at  $60^{\circ}$ N. The SCE data during the first week in December 2020 are plotted in Fig. 1.

Thorough descriptions of the data are provided in Dye (2002) and Estilow et al. (2015). Early discussion of the data's production is found in Wiesnet et al. (1987) and Robinson et al. (1993). Before June of 1999, NOAA used the first clear-sky day during each week to estimate the SCE. If the cell contains at least 50% snow coverage, its SCE was assigned as unity; otherwise, it is assigned zero.

With the introduction of the Interactive Multisensor Snow and Ice Mapping System (IMS), the methods used to estimate



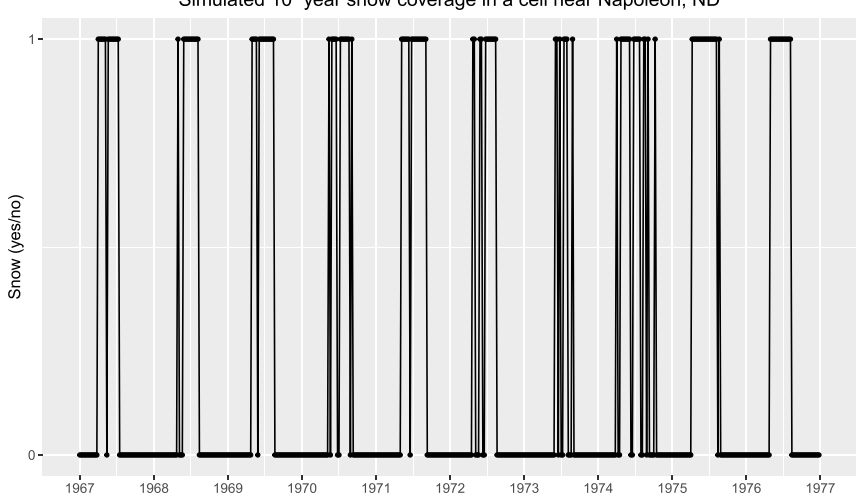


FIG. 2. (top) Ten years of snow presences/absences (August 1967–July 1976) for a cell near Napoleon, ND (46.4309°N, 99.8852°W). (bottom) Ten years (August 1967–July 1976) of simulated data. This simulation is discussed in section 5. In both graphics, the yearly tick marks refer to 1 Aug of each calendar year, employing a winter-centered year paradigm.

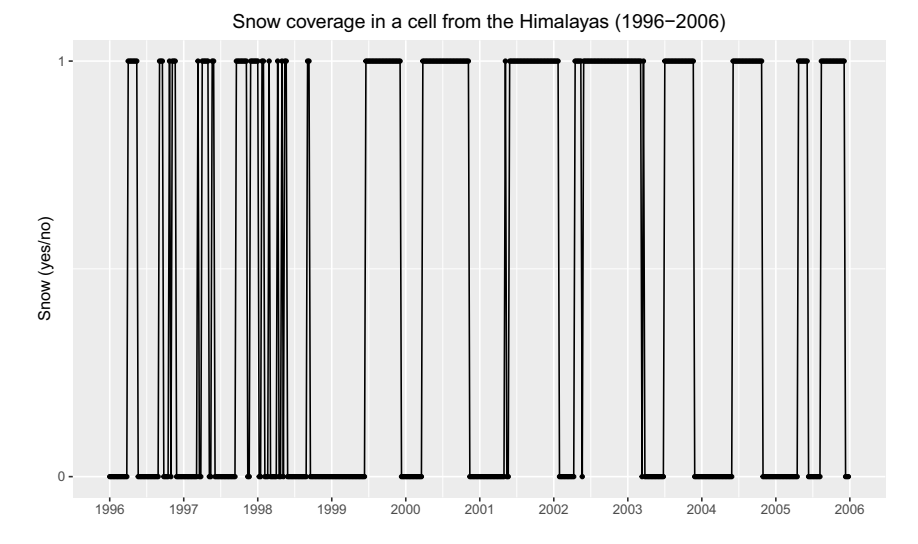
SCE changed in June 1999. These methods use different data and a refined grid partition of 24 km covering the NH to estimate snow presence/absence on the 190.4-km resolution grid; these changes are detailed in Estilow et al. (2015). Brown et al. (2007) did not find evidence of inhomogeneities over northern Canada before and after the 1999 change; however, Déry and Brown (2007) claim that pre-1999 methods overestimate snow presence in mountainous regions during spring ablation. An analysis of the 1999 changes is provided later.

There are other changes in the data construction procedure Estilow et al. (2015) for the data product studied here. In June of 1977, the Defense Meteorological Satellite Program data supplemented the data record. Next, Geostationary Meteorological Satellite imagery was introduced to the data construction in February of 1988 and January 1989. In May of 1999, the IMS system was

introduced into the data construction process. Finally, NOAA took over responsibility of data construction in June of 2008.

Ten years of observations for a cell located near Napoleon, North Dakota (46.4309°N, 99.8852°W), from August 1967 to July 1976 are displayed in Fig. 2. This cell will be analyzed in detail in section 5. The graph reveals the ephemeral nature of snow processes here, starting each year circa November and typically lasting through early April. Once snow cover is present, it usually stays through spring ablation; however, years exist when snow is absent midwinter (1967/68 and 1973/74, for examples).

The data in this study contain 7744 NH cells, 3011 of which are deemed to be over land. See the metadata for the key to this partition, or to obtain cell areas. Winter-centered years are used here so that the first week of any year corresponds to the first week of August. This scaling prevents a single winter's snow record from



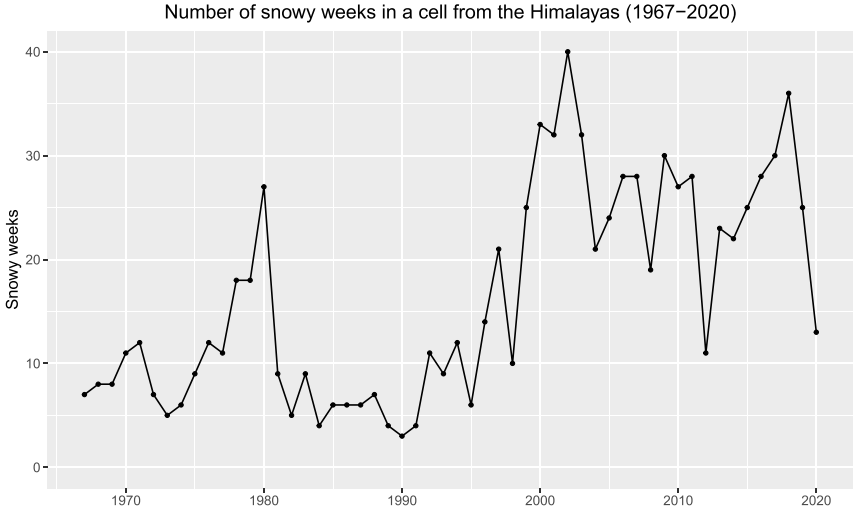


FIG. 3. A cell from the Himalayas  $(27.9682^{\circ}N, 97.7094^{\circ}E)$  with untrustable data. (top) Ten years of snow presence/absence from August 1996 to July 2006. Tick marks are placed at 1 Aug of each calendar year. (bottom) The number of snow-covered weeks during the 1967–2020 period. Tick marks are placed at 1 Aug of each calendar year.

lying within two distinct years. Shifting in this manner is done for convenience only—the scaling does not influence any trends.

# Data preprocessing

Before beginning any analysis, each land cell was categorized into four subgroups, depending on its data. Group 1 includes all cells that reported 10 or fewer weeks of snow cover during the 1967–2020 period of record (2808 weeks). This group also contains any cell that reported 10 or fewer weeks of bare ground over the record period. Group 1 cells primarily lie in the southerly latitudes of the NH, which rarely experience snow, or the interior Greenland icecap, which is almost always under snow cover. All 1131 Group 1 cells were excluded as any trends computed from these records lack sufficient information/variability to fit our model (there are more model parameters than changes in snow presence/absence).

Group 2 contains 72 cells that were insufficiently fitted by our model (our model is the subject of the next section). While these cells all had more than 10 snow/bare ground weeks during the 2808 week study period, they typically did not have many more. While one can theoretically obtain trend estimates for cells in Group 2, error margins obtained are so large that any trend estimates would essentially be meaningless. These cells were primarily located in southern China, the southern United States, and coastal Greenland. While one could combine Group 1 and Group 2 together into a single "insufficient information" group, we keep the groups separate on this technical distinction: trend error margins do not exist in Group 1, and while they exist for Group 2, they are too large to make any conclusions.

Several studies (Bormann et al. 2018; Estilow et al. 2015) discuss the unreliable snow presence/absence estimates in

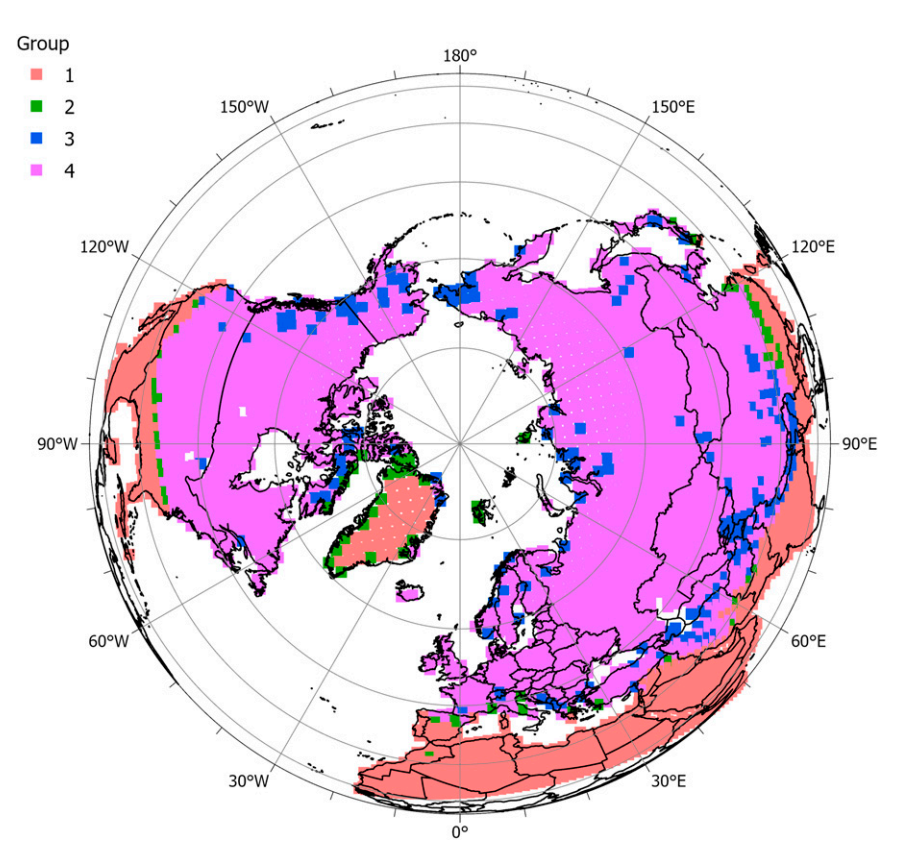


FIG. 4. A graphical partition of this studies' cell groups. The violet colored cells (Group 4) were deemed analyzable. Group 1 cells are excluded because there are not enough changes from presence to absence (or vice versa) to fit our model. Group 3 cells were excluded as their data were deemed unreliable by our quality control methods, which agrees with the findings of other authors. Group 2 contains a small number of cells whereby the standard errors of the trend estimates are so large as to make any trend estimates untrustable.

mountainous regions in the pre-1999 data. Figure 3 plots the data from an example Group 3 cell located in the Chinese Himalayan mountain range near 27.9682°N, 97.7094°E. Several issues are apparent. The top plot shows that some of the earlier years in the record have no snow cover in winter weeks, but some snow cover during summer weeks. The bottom plot reveals that the pre-1999 years report very little snow cover compared to the post-1999 years. While the methodological revisions in 1999 may render the post-1999 data believable, this cell is best excluded in a trend analysis. As such, our immediate objective is to construct a quality control method to be applied to all cells before trend analysis.

Let  $\{X_t\}$  denote the two-state snow presence/absence series in time. Here,  $X_t = 1$  means that snow cover is present at time t and  $X_t = 0$  means that snow is absent at time t. Let  $S_n$  be the number of weeks of snow on the ground during year n:

$$S_n = \sum_{\nu=1}^T 1_{[X_{(n-1)T+\nu}=1]},$$

where  $1_A$  denotes the indicator of the event A and T = 52 is the period of the data.

As a quality control measure, a traditional cumulative sum (CUSUM) test statistic is applied to  $\{S_n\}$  from each land cell

not in Groups 1 or 2. The CUSUM statistic has been widely used for statistical quality control for more than 50 years (Bissell 1969). The CUSUM method checks for structural breaks in the  $\{S_n\}$  data series. The significance level for the test was set to  $1 \times 10^{-5}$ . If the CUSUM statistic for the cell has a p value less than this significance level, the cell is deemed corrupted and is classified as belonging to Group 3.

Group 3 contains 190 cells. These cells overwhelmingly reside in the mountainous regions of the NH (Rockies, Alps, Caucasus, Scandinavia, and Himalayas) and are omitted from further analysis. The discarded cells largely align with the regions discussed in Bormann et al. (2018). Our CUSUM analysis addresses a point raised in Estilow et al. (2015): "More research is needed to determine whether SCE analysis in mountainous regions (e.g., the Tibetan Plateau) shows systematic change during this time period." We concur with Bormann et al. (2018): the analysis in the Tibetan and other high mountain regions changed with the implementation of the IMS based product in May of 1999. The data before 1999 are unreliable in many high mountain regions.

Figure 4 depicts the group category of all cells; there are 1618 violet-shaded cells where our model fit was deemed reliable. These cells cover most areas of the NH where snow is

seasonally persistent. A spreadsheet containing the group numbers of our cells, and all code used for this project, is available at <a href="https://github.com/JiajieKong/Snow-Presence-Trends">https://github.com/JiajieKong/Snow-Presence-Trends</a>.

Several previous studies of these data exist. Déry and Brown (2007) studies the data from January 1972 to December 2006. Déry and Brown (2007) report significant temporal autocorrelation in the data, at both weekly and annual scales. Autocorrelation makes some statistical methods such as Sen's slope troublesome for trend analysis as uncertainties are extremely difficult to estimate with such a nonparametric method (Yue et al. 2002). Negative trends in SCE area are reported in Déry and Brown (2007) from March through June. Figure 4.3 in Lemke et al. (2007) shows March–April snow cover departures by subtracting the percentage coverage (by cell) of weeks with snow cover from 1988 to 2004 minus the same percentage coverage during 1967-87. While it is not clear how to interpret such a statistic as any type of smooth trend, the largest reductions in that study occurred roughly between the 0° and 5°C isotherms.

## 3. Model and estimation

#### a. The model

Our methods use a two-state Markov chain model on the states  $\{0, 1\}$  to describe the series for a fixed cell. This model can accurately quantify trend uncertainty as shown below. State zero indicates lack of snow and state one signifies snow cover. The transition probability matrix of this chain from week t-1 to week t is parameterized as

$$\mathbf{P}(t) = \begin{bmatrix} p_{0,0}(t) & p_{0,1}(t) \\ p_{1,0}(t) & p_{1,1}(t) \end{bmatrix}.$$

Here,  $p_{0,1}(t)$  is the probability that snow cover is present at time t given that it is absent at time t-1. The other three elements in the matrix are similarly interpreted. There are only two free quantities in  $\mathbf{P}(t)$  at any t since  $p_{0,0}(t) = 1 - p_{0,1}(t)$  and  $p_{1,0}(t) = 1 - p_{1,1}(t)$ .

The marginal probability distribution of  $X_t$  at time t will be denoted by  $\pi(t) = [\pi_0(t), \pi_1(t)] = [P(X_t = 0), P(X_t = 1)]$ . Because the chain commences with an observation in August, the startup condition  $\pi(1) = (1, 0)$  is taken, signifying that the chain starts with bare ground. With this initial distribution,  $\pi(t)$  is computed via

$$\boldsymbol{\pi}(t) = \boldsymbol{\pi}(1) \prod_{k=2}^{t} \mathbf{P}(k). \tag{1}$$

For each pair of times  $t_1 < t_2$  in  $\{1, ..., N\}$ , the transition matrix

$$\mathbf{P}^*(t_1, t_2) = \prod_{t=t_1+1}^{t_2} \mathbf{P}(t)$$

contains the four transition probabilities of snow cover/ absence from time  $t_1$  to time  $t_2$ .

Since  $p_{0,1}(t)$  and  $p_{1,0}(t)$  are probabilities, they take values in [0, 1]. Hence, these quantities are modeled with the logistic-type link

$$p_{0,1}(t) = \frac{1}{1 + \exp(-m_t)}, \quad p_{1,0}(t) = \frac{1}{1 + \exp(-m_t^*)},$$

where  $m_t$  and  $m_t^*$  contain seasonal effects and trend parameters. These quantities are posited to have the additive form

$$m_t = \mu_t + \alpha t, \quad m_t^* = \mu_t^* + \alpha^* t,$$

where the parameters are clarified as follows. For the weekly observations analyzed here, the period T=52 weeks is forced to the data by omitting any observations that occur at the end of July (one day during nonleap years and two days during leap years). This tactic results in little loss of precision; see Lund et al. (2006) for similar tactics. The parameters  $\mu_t$  and  $\mu_t^*$  contain seasonal effects that are sinusoidaly parameterized

$$\mu_t = A_0 + A_1 \left\{ \cos \left[ \frac{2\pi(t-\tau)}{T} \right] \right\},$$

$$\mu_t^* = A_0^* + A_1^* \left\{ \cos \left[ \frac{2\pi(t - \tau^*)}{T} \right] \right\}.$$

Observe that  $\mu_t$  and  $\mu_t^*$  are periodic with period T = 52 weeks and obey  $\mu_{t+T} = \mu_t$  and  $\mu_{t+T}^* = \mu_t^*$ . The quantities  $A_0$  and  $A_0^*$ govern the length of the snow season. For example, when  $A_0 > 0$ , the season where snow is present tends to last longer than the snow free season (and vice versa). The parameters  $A_1$  and  $A_1^*$ , which are assumed positive for mathematical identifiability of the cosine waves, control how fast snow to bare ground transitions take place (and vice versa). The parameters  $\tau$  and  $\tau^*$  are phase shifts. Since  $p_{0.1}(t)$  and/or  $p_{1.0}(t)$  are maximized when  $m_t$  and/or  $m_t^*$  is maximized, and the cosine function is maximized when its argument is zero,  $p_{0,1}(t)$  is maximized at week  $\tau$ , which is typically in the late fall or early winter, and  $p_{1.0}(t)$  is maximized at week  $\tau^*$ , which typically occurs in the late winter or early spring. The parameters  $\alpha$  and  $\alpha^*$  are linear trend parameters and govern how fast snow cover changes are happening. While the above model has a linear time trend and a simple cosine seasonal cycle, other forms of trends and seasonality could be used if needed.

Our periodic Markov chain model allows  $X_t$  to be autocorrelated in time t. Indeed, week-to-week SCE data exhibit correlation: if snow is present/absent at week t, it is more likely to be present/absent at week t+1. Good models for snow depth processes are also correlated in time. Indeed, Woody et al. (2009) argues for a Markov structured storage model for daily snow depths: the snow depth today is the snow depth yesterday, plus any new snowfall, minus any meltoff or compaction between yesterday and today. Our model is not a classical Probit count time series model as these are typically used for uncorrelated data; see Chib and Greenberg (1998) for more on probit modeling. A Markov model for binary data is parsimonious in that there are only two free parameters in  $\mathbf{P}(t)$  for each fixed t. While seasonal and trend features need

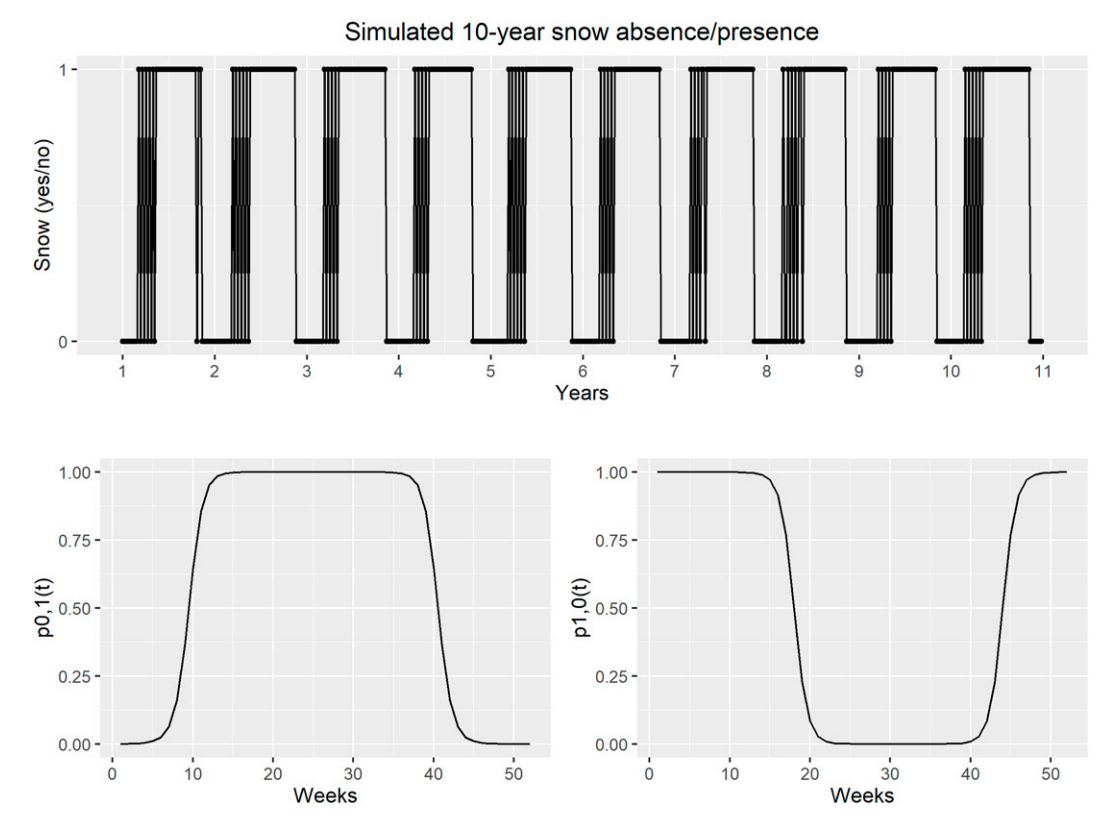


FIG. 5. A simulated 10-yr snow absence/presence series with plots of the transition probabilities  $p_{0,1}(t)$  and  $p_{1,0}(t)$ . The parameters are  $A_0 = 3$ ,  $A_1 = 10$ ,  $\tau = 25$ ,  $\alpha = 0$ , and  $A_0^* = 0$ ,  $A_1^* = 10$ ,  $\tau^* = 5$ ,  $\alpha^* = 0$  (no trend).

to be incorporated into  $\mathbf{P}(t)$  to handle the periodic nature of snow, the overall model is very parsimonious. Comparing further, a time homogeneous Markov model for categorical sequences taking on S distinct categories has S(S-1) free parameters, which is quite large for a large S. Additional parameters would be needed to make this model periodic.

Figure 5 shows a simulation of ten years of a binary snow presence process. The parameters chosen for  $p_{0,1}(t)$  are  $A_0 = 3$ ,  $A_1 = 10$ ,  $\tau = 25$ ,  $\alpha = 0$ , and those for  $p_{1,0}(t)$  are  $A_0^* = 0$ ,  $A_1^* = 10$ ,  $\tau^* = 5$ ,  $\alpha^* = 0$ ; specifically, there is no trend in the simulated data. One sees that each and every year, snow presence begins in the fall and stays on the ground until spring, oscillations between seasonal snow presence and bare ground occur in the fall, and snow vanishes completely during the summer. Additional simulations show that this simple Markov chain model produces a flexible suite of snow presence/absence series.

#### b. Parameter estimation

Suppose that the data sample  $\mathbf{X} = (X_1, \dots, X_N)'$  is available for a cell. We assume that N is a multiple of T to avoid trite work with fractional portion of years; this said, the methods are easily modified to accommodate fractional parts of years if needed. Let d = N/T denote the total number of years of observations; we work with observations indexed as the years  $1, 2, \dots, d$ .

Let  $\Theta$  denote all model parameters contained in  $m_t$  and  $m_t^*$ . These include  $A_0$ ,  $A_1$ ,  $\tau$ ,  $\alpha$  and their starred counterparts. The statistical likelihood of  $\Theta$ , denoted by  $L(\Theta|\mathbf{X})$ , can be derived from the Markov property and is

$$\ln[L(\mathbf{\Theta}|\mathbf{X})] = \sum_{t=2}^{N} \ln[p_{X_{t-1}, X_t}(t)].$$
 (2)

The quantities  $p_{i,j}(t)$  depend on  $\Theta$ . Numerically maximizing this likelihood is the classical statistical way of estimated the components in  $\Theta$ ; that is, likelihood estimates model parameters as those that make the observed data most likely. These estimates will be used later in assessing variability (uncertainty) margins of the trends. The data  $X_1, \ldots, X_N$  are held fixed in this maximization. While explicit forms for the estimators of the components in  $\Theta$  do not exist, likelihood estimates can be obtained numerically. The R programming language version 4.1.2 was used for all statistical coding in this study, the numerical routine "optim" was employed for optimization in this study.

# c. Trend estimation and their uncertainties

Trends will be phrased in the number of snow days lost/gained per decade. For example, future trends will be phrased as a loss of one day of annual snow cover over a decade. Trends are estimated directly from the data product for all

Group 4 cells. The linear rate of SCE change is quantified by  $\hat{\beta}$  defined by

$$\hat{\beta} = \frac{\sum_{k=1}^{d} S_k(k - \overline{k})}{\sum_{k=1}^{d} (k - \overline{k})^2} = \frac{\sum_{k=1}^{d} S_k(k - \overline{k})}{Q},$$
(3)

where  $\overline{k} = (d+1)/2$  is the average time index and the denominator can be verified as Q = d(d+1)(d-1)/12. While the units of  $\beta$  are weeks of snow cover gained/lost per year, we will scale  $\hat{\beta}$  to days of snow cover gained/lost per decade for interpretability; this simply multiplies raw trends and their standard errors by 70.

Our next objective is to obtain a standard error for  $\hat{\beta}$ . Taking a variance in (3) gives

$$\operatorname{Var}(\hat{\boldsymbol{\beta}}) = \frac{\sum_{k=1}^{d} \sum_{\ell=1}^{d} (k - \overline{k})(\ell - \overline{k}) \operatorname{Var}(S_k, S_{\ell})}{O^2}.$$

This computation requires  $\operatorname{Cov}(S_n, S_{n+h})$  for every h > 0 and n in  $\{1, \ldots, d-h\}$ . Details for this computation are provided in the appendix. The standard error of  $\hat{\beta}$  accounts for any correlation in the SCE data.

To statistically test whether or not SCE is changing, we want to test the null hypothesis that  $\beta = 0$  against the alternative that  $\beta \neq 0$ . Invoking asymptotic normality of the estimator  $\hat{\beta}$ , this is assessed through the Z-score statistic

$$Z = \frac{\hat{\beta}}{\operatorname{Var}(\hat{\beta})^{1/2}},$$

which is compared to the standard normal distribution to make conclusions. One typically reports a *p* value for the test to assess significance of the trends; this is illustrated further in section 6.

# 4. A simulation study

This section studies our model and estimation procedure via simulation, illustrating the model's capabilities and how parameters are estimated.

To demonstrate the model's flexibility, Fig. 6 provides 10-yr sample plots of snow presence/absence series generated by models for five sets of parameter values. Only 10 years of data are shown as it becomes visually difficult to see data features with longer series (the plot becomes "compressed"). Table 1 lists all parameters considered. The unstarred parameters govern  $p_{0,1}(t)$ , which controls transitions from bare ground to snow cover; the starred parameters govern  $p_{1,0}(t)$ , which controls transitions from snow cover to bare ground.

Models I–V have no trend. Models with trends will be considered below. The parameters for Model I were chosen to represent a scenario that is seasonally regular, with snow cover becoming present in the late fall and staying until spring ablation. The parameters  $A_0$  and  $A_0^*$  are set to zero, making the winter "snow season" last roughly half the year. Model II

has the same parameters as Model I, except that  $\tau^*$  was changed from 0 to 42, shifting the cosine wave governing  $p_{1,0}(t)$  from its Model I settings. This change makes both  $p_{0,1}(t)$  and  $p_{1,0}(t)$  relatively large during the spring months, which induces a spring SCE season that oscillates more frequently between bare ground and snow cover. Model III has the same parameters as Model I, except that  $\tau$  was changed from 25 to 20, making both  $p_{0,1}(t)$  and  $p_{1,0}(t)$  large during the fall. This makes bare ground to snow cover oscillations more common in the fall. While we do not illustrate it here, increasing  $A_1$  or  $A_1^*$  makes "transitions" from winter to summer (and vice versa) shorter (sharper). The parameters in Model IV are set to a lower-latitude setting where snow only occurs sporadically during the middle of winter. This was done by decreasing the  $A_0$  parameter from 0 to -30 for  $p_{0,1}(t)$  and increasing  $A_1^*$ from 0 to 30 (compared to Model I). Model V's parameters correspond to a high-latitude case where snow cover is present most of the year. This was done by increasing  $A_1$  from 0 to 30 and decreasing  $A_1^*$  from 0 to -30 (compared to Model I). These and other simulations show that the model can generate a wide range of SCE patterns.

To illustrate trend features, we choose parameters that bring Model IV above to a very snowy setting, and Model V above to a nonsnowy scenario. These are done over a 1000-yr time period. These scenarios are not climatologically realistic but were chosen to demonstrate the overall flexibility of the approach. Figure 7 plots

$$\frac{1}{T} \sum_{\nu=1}^{T} X_{(k-1)T+\nu}$$

against the annual index k. This quantity is the proportion of days of year k where snow cover is present. The top graphic in Fig. 7 corresponds to Model IV, except that  $\alpha$  was changed from zero to 0.001 and  $\alpha^*$  is changed from zero to -0.001. Here, the proportion of snow covered days rises from almost zero to approximately 80%. The antipodal scenario is illustrated in the bottom graphic of this figure. This moves a very snowy location to one with infrequent snow cover. This was done by taking Model V's parameters but changing  $\alpha$  from 0 to -0.001 and  $\alpha^*$  from 0 to 0.001.

Turning to estimation, our first simulation case studies a 50-yr series (N=2600), which is roughly the length of the data studied here. The parameters chosen for this simulation are those for Model I above; there is no trend in these simulations. These parameters were chosen to correspond to fitted parameters in some of our cells. Figure 8 shows violin plots of the eight parameter estimators aggregated from 1000 independent simulations. The solid line in each violin plot demarcates the median of the 1000 estimators for that parameter. One sees little bias in the estimators. Specifically, the estimation procedure was able to discern that there was no trend in the series. Additional simulations (not shown here) indicate that any estimator bias recedes with increasing series length. Estimation of the eight model parameters by likelihood appears to work well in this case.

Our second simulation moves to a case with trends. This simulation takes the same series length and parameters as the

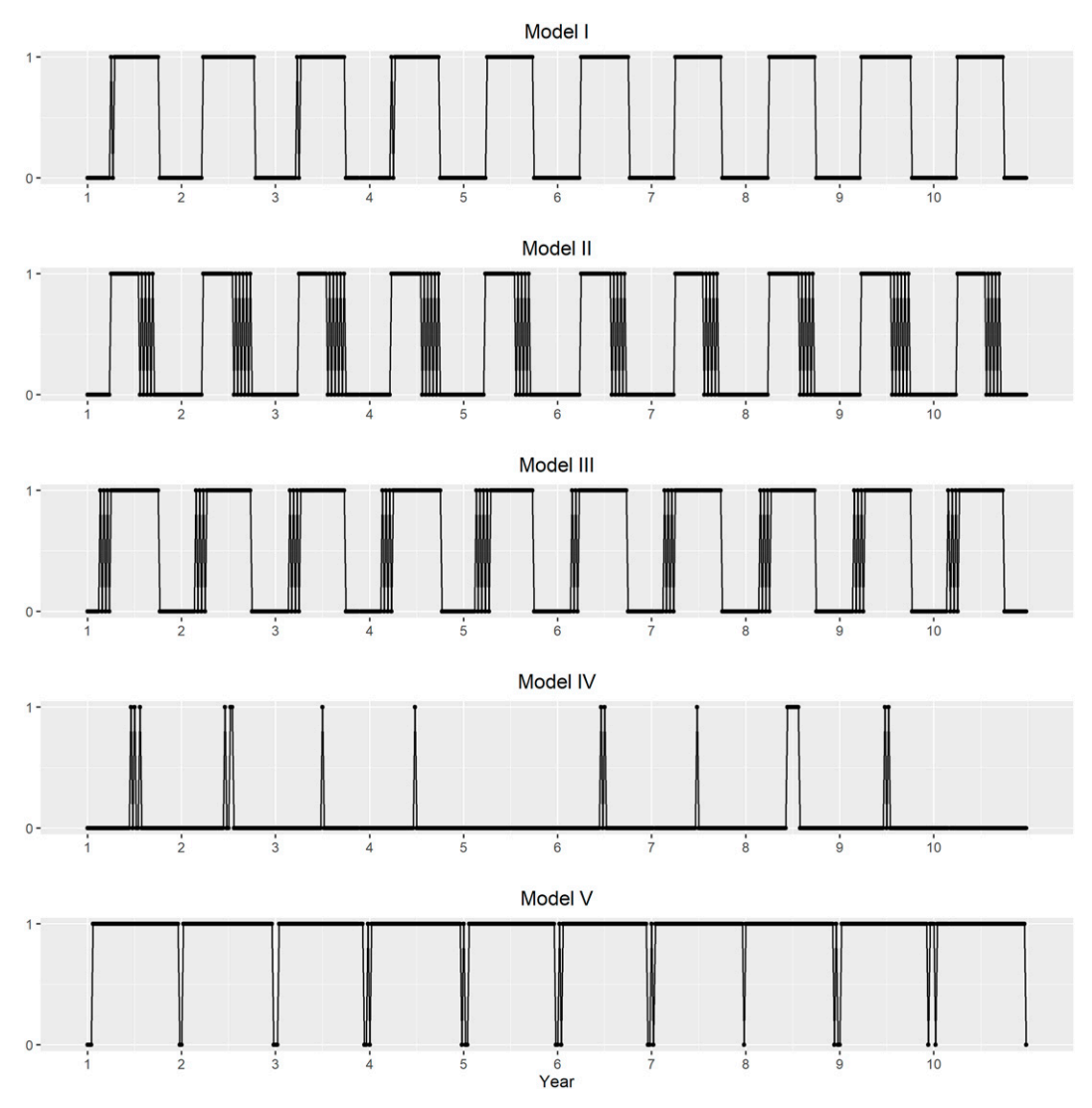


FIG. 6. Ten-year sample SCE series generated from Models I-V.

above simulation but modifies the trend parameters to  $\alpha = 0.001$  and  $\alpha^* = -0.001$ . All parameters are fixed for the duration of the series. Figure 9 shows violin plots of the estimates of each parameter and are again quite good; importantly, trend parameters

TABLE 1. Model 1 is the base case: equal transitions from no snow to snow in both fall and spring. Model II allows for more variability in the spring snow presences. Model III allows more variability in the fall snow presences. Model IV is for a cell that rarely experiences snow; Model V describes a very snowy cell.

Sample simulated series								
Model	$A_0$	$A_1$	au	α	$A_0^*$	$A_1^*$	$ au^*$	$lpha^*$
I	0	30	25	0	0	30	0	0
II	0	30	25	0	0	30	42	0
III	0	30	20	0	0	30	0	0
IV	-30	30	25	0	30	30	0	0
V	30	30	25	0	-30	30	0	0

are accurately estimated. While the trend parameters are small in magnitude in this simulation, they will be converted to days of snow cover gained/lost per decade later for ease of interpretability. Overall, the model parameters are reasonably accurately estimated with 50 years of weekly data.

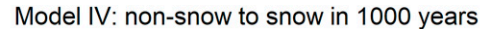
#### 5. A sample cell

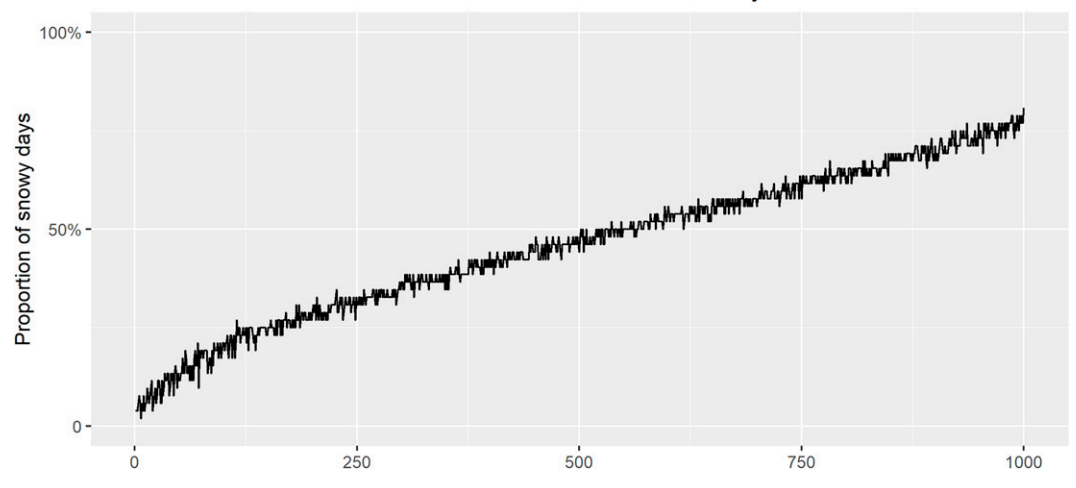
This section analyzes snow coverage in a cell near Napoleon, North Dakota (46.4309°N, 99.8852°W). This cell contains a region studied in Woody et al. (2009).

In the ensuing analysis, our null hypothesis is that the snow presence/absence series is not changing. This corresponds to the null hypothesis

$$H_0: \alpha = \alpha^* = 0,$$

with the alternative hypothesis being that SCE is changing.





# Model V: snow to non-snow in 1000 years

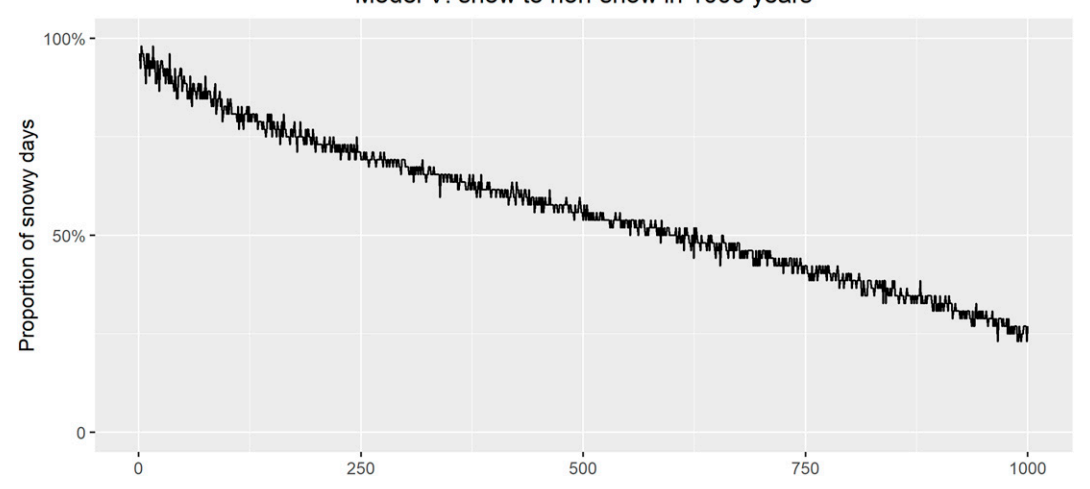


FIG. 7. Annual proportions of snowy days from Models IV and V with nonzero trends.

Table 2 below shows the maximum likelihood estimates of the parameters in the section 3 model along with a single standard error. All estimated parameters appear significantly nonzero except for the  $\alpha$  parameters (one does not usually assess whether or not the phase shift parameters  $\tau$  and  $\tau^*$  are zero). Statistical significance is assessed using asymptotic normality. There is no statistical evidence to conclude that  $\alpha$  is different from zero with a p value of 0.7708, and we conclude that  $p_{0,1}(t)$  is not changing. As  $p_{0,1}(t)$  governs transitions from bare ground to snow cover, this implies that the snow season is starting about the same time and has not changed over the study. In contrast,  $\alpha^*$  is concluded to be significantly negative with a p value of 0.0001. A negative  $\alpha^*$  makes  $p_{1,0}(t)$  smaller, which makes it harder for snow to disappear when it is on the ground. This translates to a later spring ablation.

To assess changes in the snow presences, the  $\hat{\beta}$  statistic in (3) is  $\hat{\beta} = 0.038\,613$  and  $Var(\hat{\beta})^{1/2} = 0.0247$ . This translates to an additional 2.702 days of SCE over a decade. The test statistic for changing SCE is Z = 1.5633, which has a two-sided

p value of 0.1180. This p value is insignificant for a standard 5% test, but is borderline significant for a 10% test. Conclusions may change further if one-sided alternative hypotheses are considered. The Napoleon cell is experiencing increasing (and not decreasing) SCE changes.

The top panel of Fig. 2 displays a 10-yr plot of weekly snow presence/absence values at the Napoleon cell. The bottom panel depicts data simulated from our model with the parameter estimates displayed in Table 2. Both series are of length 10 years, starting on 1 August 1967 and continuing through 31 July 1976. Visual inspection of the top and bottom panels of Fig. 2 indicates the simulated data appear to model the real data quite well.

## 6. Results

This section reports results for the 1618 cells where our model fit was deemed reliable. Figure 10 spatially portrays the trends  $\hat{\beta}$  over all analyzed cells. The corresponding Z scores

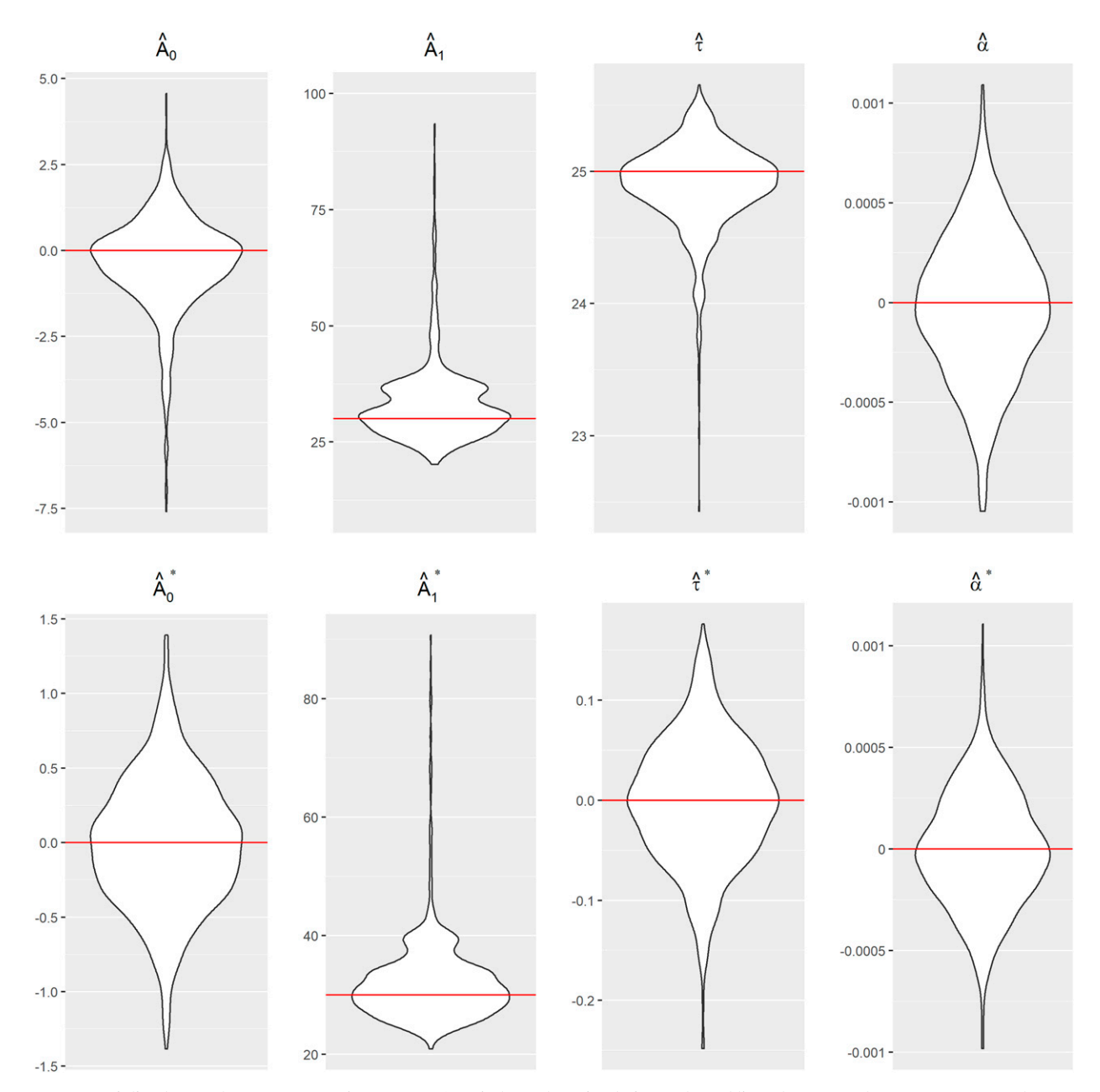


FIG. 8. Violin plots of the parameter estimates from 1000 independent simulations. The red lines demarcate the true parameter values.

for the trend statistics are displayed in Fig. 11. In totality, 573 of the cells (35.41%) report a positive  $\hat{\beta}$  (increasing snow), while 1045 cells (64.58%) show a negative  $\hat{\beta}$ . This is almost a 2 to 1 margin preference for declining to advancing snow cover. The average trend over the 1618 analyzed cells has lost 1.522 days of snow cover per decade.

Examination of the spatial structure in Figs. 10, 11, and 15 reveals regions of increasing and decreasing snow presence. Decreasing snow presence in the Arctic, particularly in Russia and western Canada and Alaska, is seen, agreeing with the findings of Bormann et al. (2018) and Estilow et al. (2015). Increasing snow is encountered in eastern Canada, the Kamchatka

Peninsula, and Japan. Other regions experiencing positive trends can be seen in Fig. 10. The Fig. 11 Z scores are deemed significantly nonzero should they exceed 2.0 in absolute value (the exact two-sided confidence level is 0.9544). Red colored Z scores demarcate cells where snow cover is declining with at least 97.72% confidence and blue colors depict increasing snow with at least 97.72% confidence. Overall, a general declining snow presence is seen along coastal areas and the periphery of the continental snowpack, with some inland increases in SCE, especially within North America. This pattern could be associated with a deeper snowpack within continental interiors and a shallower or patchier snowpack along its edges, leading to more

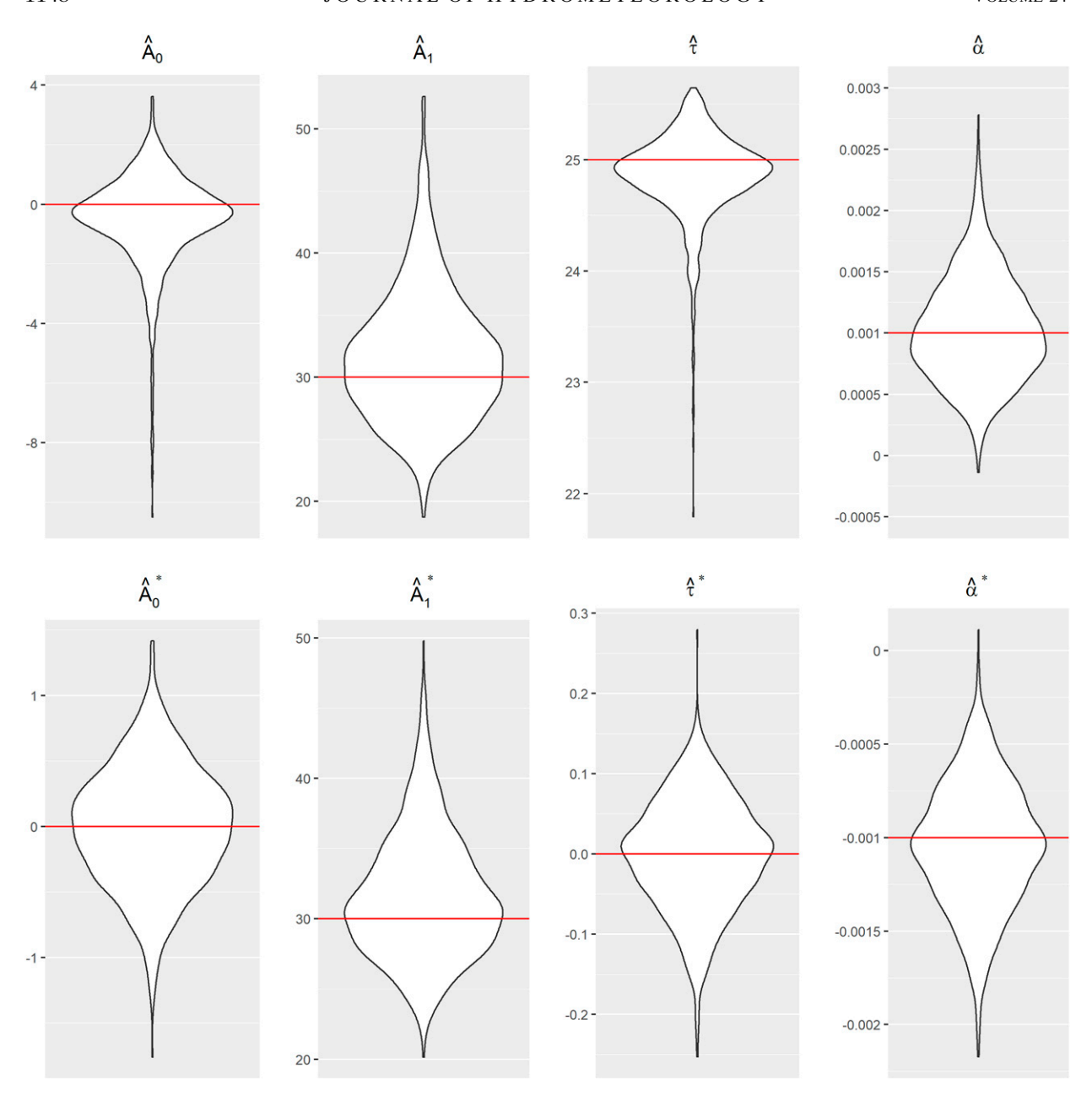


FIG. 9. Violin plots of the parameter estimates aggregated from 1000 independent simulations. The red lines demarcate the true parameter values.

rapid retreat of the snowpack and a longer duration of its center. This coincides with the finding of the fourth IPCC report in Lemke et al. (2007).

The left panel in Fig. 12 shows a histogram of the trend estimates  $\hat{\beta}$  over all analyzed cells. The estimated trends  $\hat{\beta}$  are

approximately normally distributed with a mean of -0.02174 (the loss of 1.522 days of SCE per decade alluded to above). The center and right panels in Fig. 12 show histograms of the  $\hat{\alpha}$  and  $\hat{\alpha}^*$  parameters, respectively, over these same cells. The average  $\alpha$  is -0.0004168 and the average  $\alpha^*$  is -0.0001431.

TABLE 2. Model parameter estimates and their standard errors for a cell containing Napoleon, ND.

Parameter	$A_0$	$A_1$	τ	α	$A_0^*$	$A_1^*$	$ au^*$	$\alpha^*$
Estimate	-3.2016	4.1499	24.3492	0.000 038 2	1.7258	3.7889	49.8375	-0.000 493 5
Standard error	0.2538	0.2936	0.26460	0.000 131 5	0.3774	0.4139	0.3800	0.000 127 3

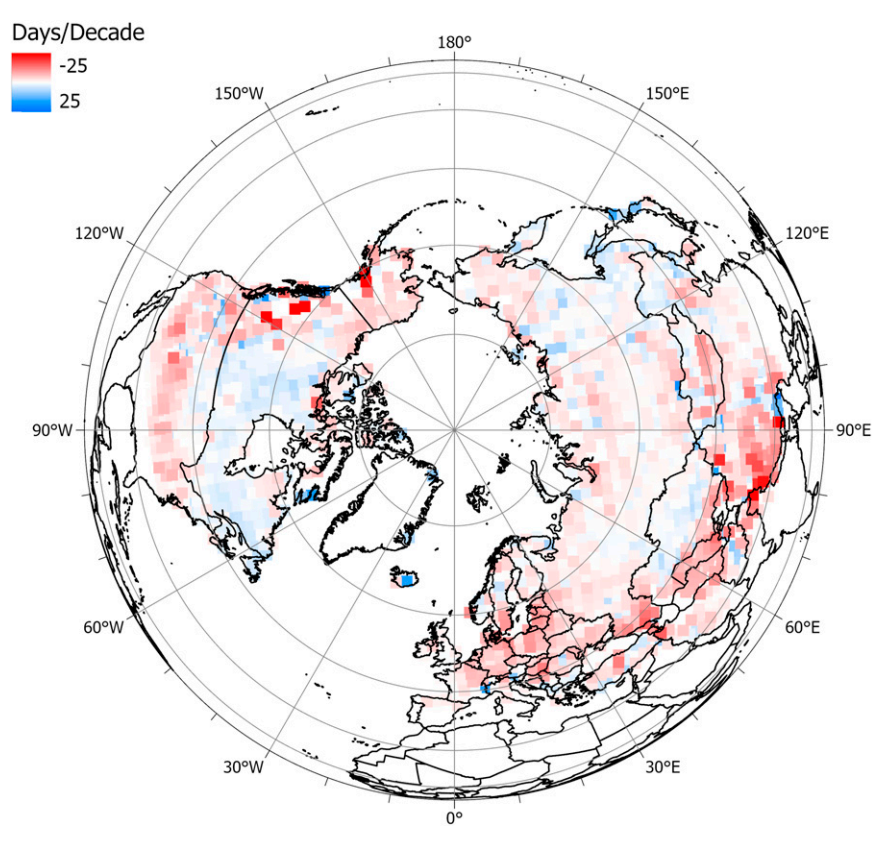


FIG. 10. Raw trends in the SCE data converted to days gained/lost per decade. Red and blue depict SCE losses and increases, respectively. Declining SCE cells outnumber advancing SCE cells by roughly a two to one ratio.

We now move to an investigation of temporal changes in the total SCE area. Figure 13 plots the total snow covered area in each week of the study over all analyzed cells. Areas were obtained by adding the area of all snow covered cells; cell areas are included with metadata (Robinson et al. 2012).

The seasonal cycle of SCE is evident, with winter weeks having the most prevalent snow cover. While interannual variability is apparent, changes in this series are not visually evident in a visual inspection.

The Fig. 13 series is denoted by  $\{G_t\}$  and is now analyzed with a periodic linear regression. More on periodic regression analyses can be found in Lund et al. (1995) and Lund (2006). Our regression model for  $G_t$  at time  $t = nT + \nu$  is

$$G_{nT+\nu} = \mu_{\nu} + \beta_{\nu} |(nT+\nu)| + \epsilon_{nT+\nu}. \tag{4}$$

The parameter  $\beta_{\nu}$  quantifies the linear rate of change in data during the  $\nu$ th week, for  $1 \le \nu \le 52$ ;  $\mu_{\nu}$  is a location parameter for week  $\nu$ . The trend slope  $\beta_{\nu}$  is allowed to depend on the week of year  $\nu$ , enabling us to investigate changes within a calendar year. The regression errors  $\{\epsilon_i\}$  are assumed to have a zero mean for every week  $\nu$ .

The week  $\nu$  trend  $\beta_{\nu}$  can be estimated via (Lund et al. 1995)

$$\hat{\beta}_{\nu} = \frac{\sum_{n=1}^{d} (G_{nT+\nu} - \overline{G}_{\nu})(nT + \nu)}{\sum_{n=1}^{d} (nT + \nu - \overline{t}_{\nu})^{2}}.$$
 (5)

Here,  $\bar{t}_{\nu} = d^{-1} \sum_{n=1}^{d} (nT + \nu) = (d+1)T/2 + \nu$  and  $\overline{G}_{\nu} = d^{-1} \sum_{n=1}^{d} G_{nT+\nu}$ . The denominator in (5) can be worked out as  $T^2 d(d+1)(d-1)/12$ . We will not delve into standard error computations for  $\hat{\beta}_{\nu}$ , but refer the interested reader to Lund et al. (2001) for more on the issue.

Figure 14 plots estimates of  $\beta_{\nu}$  against  $\nu$  for each week of year; see Lund et al. (1995) for the equations to fit this model. Increasing SCE is evident in the fall (late October through early December), with a corresponding decrease in late winter through summer. While increases span only a few months and include brief peaks above 0.5 million km², the decrease spans February–September, with losses below 0.5 million km² from May through July. This implies that while the snow season is experiencing a shift toward an earlier onset and ablation period, there is a more pronounced decrease in snow cover through the warm season that is not being offset by increased snow in the fall and early winter. Implications of this finding include a change in seasonal water availability.

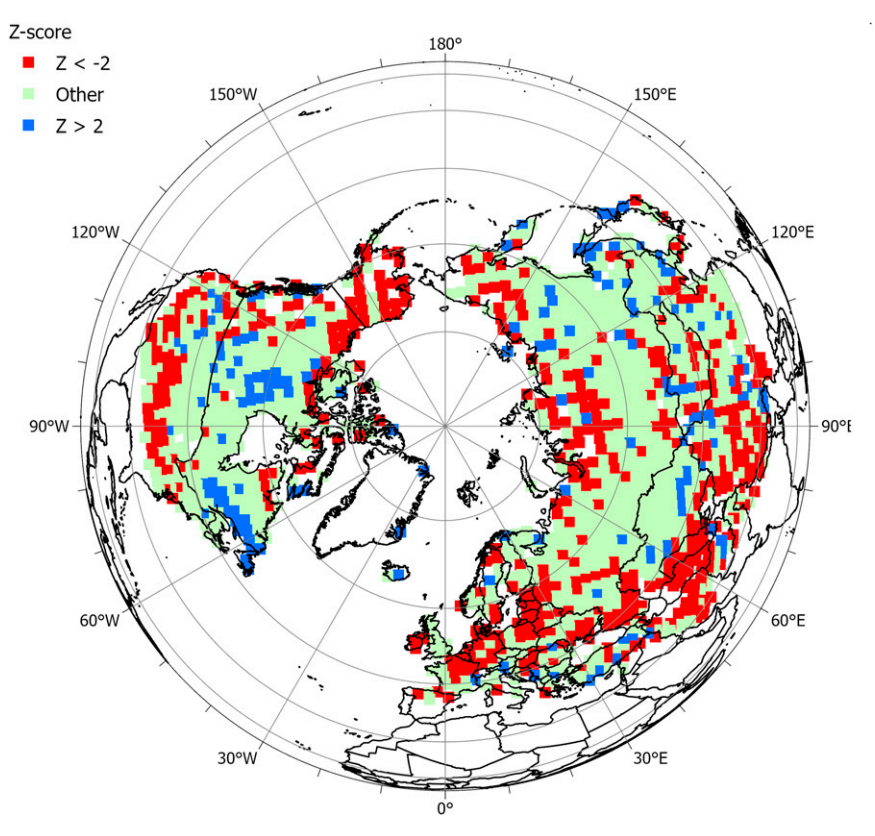


FIG. 11. Z scores of the SCE trends. Trends in around half of the cells are not significantly changing (nonzero). Red indicates declining SCE and blue increasing SCE, with one-sided confidence of at least 97.5%.

As a final task of this section, we analyze possible issues induced by the methodological changes used to extract the SCE data (these are called breakpoint times or interventions). As noted in section 2, there are five potential breakpoints in the data (Estilow et al. 2015).

Breakpoints are discontinuity features in time series that occur at known times. Breakpoints (also called interventions) often take place when measuring conditions change, such as station relocations or updates to gauge sensors. We will

investigate possible breakpoints in June 1977, February 1988, January 1989, May 1999, and June of 2008, all times where the methods to extract the zero-one SCE data changed. It would require more work to find and adjust the data for undocumented breakpoint times (called changepoints when the time of the discontinuity is unknown). Future work will assess changepoint features and homogenize the data in the individual cells. A caveat: while Lu et al. (2010) is one changepoint reference for approximately normally distributed temperature

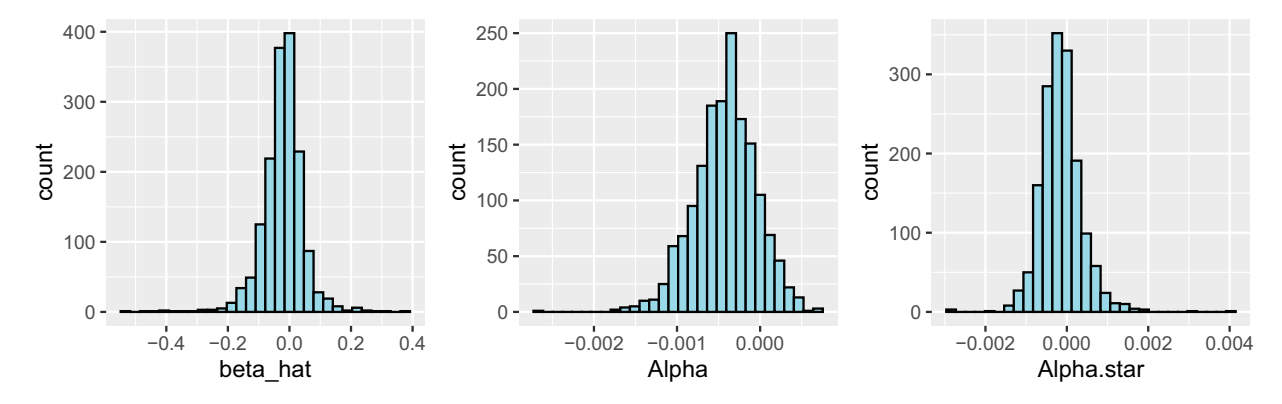


FIG. 12. Histograms over all 1618 analyzed cells of (left) the estimated SCE trends  $\hat{\beta}$ , (center) the  $\hat{\alpha}$  estimates, and (right) the  $\hat{\alpha}^*$  estimates. All histograms appear roughly unimodal (normally distributed). The mean of the left histogram is slightly negative.

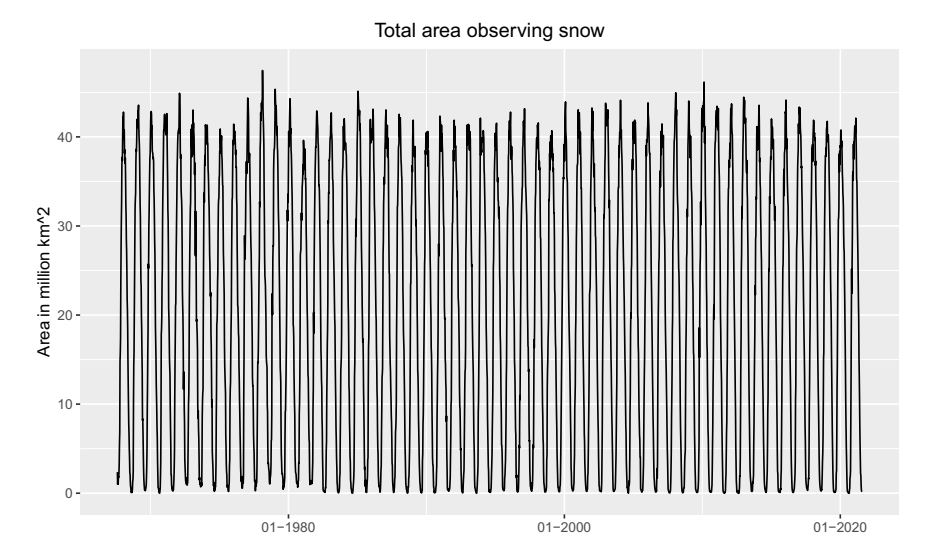


FIG. 13. Total SCE area by week over the period of record. Trends are not visually obvious.

data, methods to homogenize zero-one count data have yet to be developed (or have not matured) in the statistics literature.

This will be done for the total SCE only; a deeper analysis exploring the effects on the individual cells is omitted. To conduct this analysis, shifts are allowed during June 1977, February 1988, January 1989, May 1999, and June 2008. The setting is quantified through the regression

$$G_{nT+\nu} = \mu_{\nu} + \beta_{\nu}(nT+\nu) + \sum_{i=1}^{5} \Delta_{i} 1_{(nT+\nu \ge b_{i})} + \epsilon_{nT+\nu}, \quad n = 0, 1, ..., d-1.$$
(6)

Here,  $b_1 = 515$ ,  $b_2 = 1069$ ,  $b_3 = 1117$ ,  $b_4 = 1654$ , and  $b_5 = 2126$  are the week time indexes of the June 1977,

February 1988, January 1989, May 1999, and June 2008 breakpoint times and  $\Delta_i$  is the associated shift size of the *i*th breakpoint time. We do not allow  $\Delta_i$  to depend on  $\nu$ , but could do so if desired.

Next, a backward elimination regression procedure at level 95% was conducted to eliminate insignificant breakpoint times. This procedure found the June 1977 and June 2008 breakpoints to be insignificant. The regression model was refitted with the other three breakpoints,  $\Delta_2$ ,  $\Delta_3$ , and  $\Delta_4$ . Estimates of these three shift sizes are shown in Table 3. The listed p values for these shift sizes indicate high confidence that the methodological changes impacted observations, essentially making observations "snowier." In fact, the only positive trend slopes occur from October to December after the breakpoints are taken into account.

# Snow cover area lost/gained per decade by season



FIG. 14. Seasonal trend estimates of SCE changes for each week of the year, scaled to area/gained lost per decade. Trends are larger when the February 1988, January 1989, and May 1999 breakpoints for method changes to extract the SCE data are considered.

TABLE 3. Estimates, standard errors (S.E.), and *p* values for the breakpoints in February 1988, January 1989, and May 1999.

	$\hat{\Delta}_2$ (February 1988)	$\hat{\Delta}_3$ (January 1989)	$\hat{\Delta}_4$ (May 1999)
Estimate	-1.871	1.196	0.407
S.E.	0.291	0.291	0.144
p value	$1.48 \times 10^{-10}$	$4.06 \times 10^{-5}$	0.0047

# 7. Summary and comments

This paper estimated Northern Hemispheric SCE trends over the last 54 (winter-centered) years. A flexible model was developed to quantify trends in periodic presence/absence data and assess their uncertainty margins. The SCE data were collected weekly and are count valued, taking the value of unity if snow is present and zero if snow cover is absent. The data are periodic, with snow being more prevalent in the winter weeks. A contribution of this paper is the development of a model that adequately captures the data's periodicities and count structure. Uncertainty margins of the trend estimates were developed. The model is highly flexible and could be fitted to most cells in Europe, North America, and Asia that report snow. In most of the contiguous United States, trends

could be reliably assessed down to latitudes of Prescott, Arizona; Carlsbad, New Mexico; and Knoxville, Tennessee (the exception being some questionable SCE data from cells in mountainous area).

The results show that snow cover is declining overall, by a margin of almost 2 to 1 in terms of cell numbers. Arctic localities are showing heavy snow cover loss; however, some regions are experiencing increasing snow coverage, most notably central and eastern Canada and the Kamchatka and Japan vicinity. Along with this general decline, a shift in the snow season toward an earlier onset and an earlier ablation period was seen, with the onset trending toward more snow in November and the ablation period showing declines from February through late spring and early summer. The increased ablation in the warm season is not offset by the increased snow cover in the late fall, possibly implying an overall change in the timing and distribution of water availability to regions that rely on spring snowmelt.

Statistical improvements can be made to this analysis. There is undoubtedly some nonzero spatial correlation between neighboring cells. Accounting for spatial correlation would potentially lower uncertainty margins in the trend estimates; correlation usually does not appreciably change trend estimates, but accounting for correlation in multiple similar cells could reduce uncertainty margins in the trends.

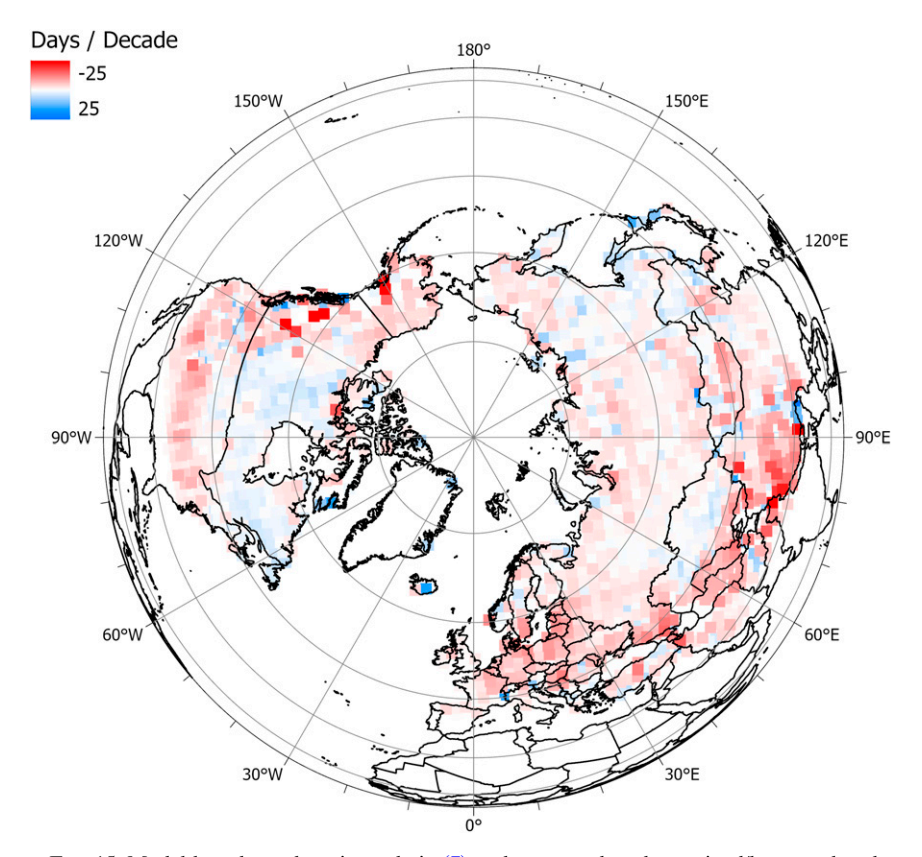


FIG. 15. Model-based trends estimated via (7) and converted to days gained/lost per decade. Red and blue depict SCE losses and increases, respectively. Declining SCE cells outnumber advancing SCE cells by roughly a two to one ratio. The graphic is similar to Fig. 10.

Given the data quality issues present, the authors felt it more prudent to analyze the cells one by one and report which ones were "unusable," which a spatial analysis would not do (at least initially). It is also possible to smooth the Fig. 10 trends and/or their Z scores in Fig. 11 in a spatial manner. We did not pursue this here due to length concerns.

The reader may note that our trend estimates are based on the data only and do not depend on the model (as it should be). This said, one can also extract a trend estimate from the model. One model-based trend is

$$\frac{E[S_n] - E[S_1]}{n - 1}. (7)$$

Both  $E[S_n]$  and  $E[S_1]$  are computed from the estimated model parameters, say computed ignoring the breakpoint. Figure 15 shows a plot of these trends, converted to days of SCE gained/lost per decade. The graphic naturally resembles Fig. 10. Differences in the estimated and modeled trends are shown in Fig. 15 and are very small overall.

While most cells report what appears to be high-quality data, the green-colored cells in Fig. 4 contain suspect data. The hope is that the data from these cells can be reexamined/fixed in the future for inclusion in studies such as this.

Acknowledgments. Robert Lund, Yisu Jia, Jiajie Kong, and Jon Woody thank NSF Grant DMS 2113592 for partial support.

Data availability statement. The Northern Hemispheric snow cover extent data in this study are available at https://www.ncei.noaa.gov/access/metadata/landing-page/bin/iso?id=gov.noaa.ncdc:C00756. The data from August 1967 to July 2021 were used here to obtain 54 complete winter-centered years.

# **APPENDIX**

## **Derivation of Variance for Eq. (3)**

We start by computing  $Cov(S_n, S_{n+h})$  for every h > 0 and n in  $\{1, \ldots, d-h\}$ . For this,  $Cov(S_n, S_{n+h}) = E[S_nS_{n+h}] - E[S_n]E[S_{n+h}]$ . To get  $E[S_n]$ , use

$$E[S_n] = E\left[\sum_{\nu=1}^T 1_{[X_{(n-1)T+\nu}=1]}\right] = \sum_{\nu=1}^T P[X_{(n-1)T+\nu}=1]$$
$$= \sum_{\nu=1}^T \pi_1[(n-1)T+\nu].$$

This quantity will need to be estimated/evaluated at the model's maximum likelihood parameters.

The calculation of  $E[S_nS_{n+h}]$  for h > 0 is a little more delicate. First, suppose that h > 0; the case where h = 0 will be handled separately. Then

$$\begin{split} E[S_n S_{n+h}] &= E\Bigg[\Bigg(\sum_{u=1}^T \mathbf{1}_{[X_{(n-1)T+u}=1]}\Bigg)\Bigg(\sum_{\nu=1}^T \mathbf{1}_{[X_{(n+h-1)T+\nu}=1]}\Bigg)\Bigg] \\ &= \sum_{u=1}^T \sum_{\nu=1}^T P[X_{(n-1)T+u} = 1 \cap X_{(n+h-1)T+\nu} = 1] \\ &= \sum_{u=1}^T \sum_{\nu=1}^T P[X_{(n-1)T+u} = 1] \\ &\times P[X_{(n+h-1)T+\nu} = 1 | X_{(n-1)T+u} = 1] \\ &= \sum_{u=1}^T \sum_{\nu=1}^T \pi_1(t_1) \mathbf{P}^*(t_1, t_2)_{2,2}, \end{split}$$

where,  $t_1 = (n-1)T_+u$ ,  $t_2 = (n-1)T_-v$ , and the notation  $\mathbf{A}_{i,j}$  denotes the element in the *i*th row of the *j*th column of the matrix  $\mathbf{A}$ .

For the case where h = 0, direct computation yields

$$\begin{split} E[S_n^2] &= E\bigg[\sum_{u=1}^T \Big(\mathbf{1}_{[X_{(n-1)T+u}=1]}\Big)^2\bigg] \\ &+ 2E\bigg[\sum_{u=1}^T \sum_{\nu=u+1}^T \mathbf{1}_{[X_{(n-1)T+\nu}=1]} \times \mathbf{1}_{[X_{(n-1)T+\nu}=1]}\bigg] \\ &= \sum_{u=1}^T P[X_{(n-1)T+u}=1] \\ &+ 2\sum_{u=1}^T \sum_{\nu=u+1}^T P[X_{(n-1)T+u}=1 \cap X_{(n-1)T+\nu}=1] \\ &= \sum_{u=1}^T \pi_1(t_1) + 2\sum_{u=1}^T \sum_{\nu=u+1}^T \pi_1(t_1) \mathbf{P}(t_1,t_2)_{2,2} \end{split}$$

after the relation  $1_A^2 = 1_A$  is applied. Here,  $t_1 = (n-1)T + u$  and  $t_2 = (n-1)T + v$ . This calculation allows us to compute  $Cov(S_i, S_i)$  for every i and j.

### REFERENCES

Barnett, T. P., J. C. Adam, and D. P. Lettenmaier, 2005: Potential impacts of a warming climate on water availability in snowdominated regions. *Nature*, 438, 303–309, https://doi.org/10. 1038/nature04141.

Bissell, A. F., 1969: Cusum techniques for quality control. *J. Roy. Stat. Soc.*, **18C**, 1–30, https://doi.org/10.2307/2346436.

Bormann, K. J., R. D. Brown, C. Derksen, and T. H. Painter, 2018: Estimating snow-cover trends from space. *Nat. Climate Change*, 8, 924–928, https://doi.org/10.1038/s41558-018-0318-3.

Brown, R., C. Derksen, and L. Wang, 2007: Assessment of spring snow cover duration variability over northern Canada from satellite datasets. *Remote Sens. Environ.*, 111, 367–381, https://doi.org/10.1016/j.rse.2006.09.035.

Brown, R. D., and D. A. Robinson, 2011: Northern Hemisphere spring snow cover variability and change over 1922–2010 including an assessment of uncertainty. *Cryosphere*, 5, 219–229, https://doi.org/10.5194/tc-5-219-2011.

Callaghan, T. V., and Coauthors, 2011: The changing face of Arctic snow cover: A synthesis of observed and projected changes. *Ambio*, 40, 17–31, https://doi.org/10.1007/s13280-011-0212-y.

Chib, S., and E. Greenberg, 1998: Analysis of multivariate probit models. *Biometrika*, 85, 347–361, https://doi.org/10.1093/ biomet/85.2.347.

- Déry, S. J., and R. D. Brown, 2007: Recent Northern Hemisphere snow cover extent trends and implications for the snowalbedo feedback. *Geophys. Res. Lett.*, 34, L22504, https://doi. org/10.1029/2007GL031474.
- Dye, D. G., 2002: Variability and trends in the annual snow-cover cycle in Northern Hemisphere land areas, 1972–2000. *Hydrol. Processes*, 16, 3065–3077, https://doi.org/10.1002/hyp.1089.
- Estilow, T. W., A. H. Young, and D. A. Robinson, 2015: A long-term Northern Hemisphere snow cover extent data record for climate studies and monitoring. *Earth Syst. Sci. Data*, **7**, 137–142, https://doi.org/10.5194/essd-7-137-2015.
- Goudie, A. S., 2018: *Human Impact on the Natural Environment*. Wiley, 472 pp.
- Karl, T. R., J. M. Melillo, T. C. Peterson, and S. J. Hassol, 2009: Global climate change impacts in the United States. U.S. Global Change Research Program, 196 pp., https://www.nrc.gov/docs/ML1006/ML100601201.pdf.
- Lawrence, D. M., and A. G. Slater, 2010: The contribution of snow condition trends to future ground climate. *Climate Dyn.*, 34, 969–981, https://doi.org/10.1007/s00382-009-0537-4.
- Lemke, P., and Coauthors, 2007: Observations: Changes in snow, ice, and frozen ground. Climate Change 2007: The Physical Science Basis, S. Solomon et al., Eds., Cambridge University Press, 337–383.
- Liston, G. E., and C. A. Hiemstra, 2011: The changing cryosphere: Pan-Arctic snow trends (1979–2009). *J. Climate*, **24**, 5691–5712, https://doi.org/10.1175/JCLI-D-11-00081.1.
- Lu, Q., R. Lund, and T. C. M. Lee, 2010: An MDL approach to the climate segmentation problem. *Ann. Appl. Stat.*, 4, 299– 319, https://doi.org/10.1214/09-AOAS289.
- Lund, R., 2006: A seasonal analysis of riverflow trends. J. Stat. Comput. Simul., 76, 397–405, https://doi.org/10.1080/106293 60500107758.
- ——, H. Hurd, P. Bloomfield, and R. Smith, 1995: Climatological time series with periodic correlation. *J. Climate*, 8, 2787–2809, https://doi.org/10.1175/1520-0442(1995)008<2787:CTSWPC> 2.0.CO:2.
- —, L. Seymour, and K. Kafadar, 2001: Temperature trends in the United States. *Environmetrics*, **12**, 673–690, https://doi. org/10.1002/env.468.
- —, Q. Shao, and I. Basawa, 2006: Parsimonious periodic time series modeling. Aust. N. Z. J. Stat., 48, 33–47, https://doi.org/ 10.1111/j.1467-842X.2006.00423.x.

- Mote, P. W., 2003: Trends in snow water equivalent in the Pacific northwest and their climatic causes. *Geophys. Res. Lett.*, 30, 1601, https://doi.org/10.1029/2003GL017258.
- —, S. Li, D. P. Lettenmaier, M. Xiao, and R. Engel, 2018: Dramatic declines in snowpack in the western U.S. *npj Climate Atmos. Sci.*, **1**, 2, https://doi.org/10.1038/s41612-018-0012-1.
- Notarnicola, C., 2022: Overall negative trends for snow cover extent and duration in global mountain regions over 1982–2020. *Sci. Rep.*, **12**, 13731, https://doi.org/10.1038/s41598-022-16743-w.
- Robinson, D. A., K. F. Dewey, and R. R. Heim Jr., 1993: Global snow cover monitoring: An update. *Bull. Amer. Meteor. Soc.*, **74**, 1689–1696, https://doi.org/10.1175/1520-0477(1993)074<1689: GSCMAU>2.0.CO;2.
- —, T. W. Estilow, and NOAA CDR Program, 2012: NOAA Climate Data Record (CDR) of Northern Hemisphere (NH) Snow Cover Extent (SCE), version 1. NOAA National Centers for Environmental Information, accessed August 2021, https://doi.org/10.7289/V5N014G9.
- Serreze, M. C., and Coauthors, 2000: Observational evidence of recent change in the northern high-latitude environment. *Climatic Change*, 46, 159–207, https://doi.org/10.1023/A:100 5504031923.
- van Mantgem, P. J., and Coauthors, 2009: Widespread increase of tree mortality rates in the western United States. *Science*, 323, 521–524, https://doi.org/10.1126/science.1165000.
- Wiesnet, D., C. Ropelewski, G. Kukla, and D. Robinson, 1987: A discussion of the accuracy of NOAA satellite-derived global seasonal snow cover measurements. *IAHS Publ.*, 166, 291–304.
- Woody, J., R. Lund, A. J. Grundstein, and T. L. Mote, 2009: A storage model approach to the assessment of snow depth trends. Water Resour. Res., 45, W10426, https://doi.org/10. 1029/2009WR007996.
- Yue, S., P. Pilon, B. Phinney, and G. Cavadias, 2002: The influence of autocorrelation on the ability to detect trend in hydrological series. *Hydrol. Processes*, 16, 1807–1829, https://doi.org/10.1002/hyp.1095.
- Zona, D., and Coauthors, 2015: Cold season emissions dominate the Arctic tundra methane budget. *Proc. Natl. Acad. Sci. USA*, **113**, 40–45, https://doi.org/10.1073/pnas.1516017113.